



ORIGINAL RESEARCH ARTICLE

Enhancing Strength and Reducing Yield Asymmetry in Extruded AZ91 Alloy through Combined Ca and Sr Additions

Ankush S. Marodkar, Vivek Kumar Sahu, and Hemant Borkar

Submitted: 13 March 2024 / Revised: 20 May 2024 / Accepted: 21 July 2024

In the present work, the effects of combined Ca and Sr additions on the microstructure, texture and mechanical properties of hot-extruded AZ91 alloy were investigated. Moreover, a detailed characterization of the recrystallization mechanisms governing the formation of new grains and final texture in extruded base AZ91 alloy and extruded AZ91-1Ca-xSr alloys was conducted. The evolution of Al-Ca and Al-Sr precipitates and their thermal stability at 400 °C extrusion temperature is predicted by thermodynamic calculations using Thermo-Calc software. The extruded microstructure of the base AZ91 alloy reveals the presence of discontinuous dynamic recrystallized grains alongside deformed grains. In contrast, extruded AZ91-1Ca-xSr alloys exhibit fully recrystallized microstructure consisting of intermetallic Al-Ca and Al-Sr stringers elongated in the extrusion direction, forming a neckless structure of stringers. In AZ91-1Ca-xSr extrusions, Al₂Ca and Al₄Sr precipitate effectively function as sites for particle-stimulated nucleation (PSN), thereby introducing localized strain energy variations. PSN leads to the formation of nuclei with random orientations, consequently reducing the overall sharpness of the texture. Ultimately, combined addition of Ca and Sr leads to improvements in both tensile and compressive strengths, with a reduction in tension-compression yield asymmetry. The enhancement of strength of extruded AZ91-1Ca-xSr alloys is primarily attributed to precipitation strengthening and grain size reduction resulting from the addition of Ca and Sr. Compared to the existing literature on the individual addition of Ca and Sr to extruded AZ91, the combined addition of both elements demonstrates superior tensile and compressive properties.

Keywords AZ91 alloy, hot extrusion, mechanical properties, texture weakening, yield asymmetry

1. Introduction

Magnesium alloys represent a compelling choice as light-weight structural materials for applications in the automotive and aerospace sectors, primarily owing to their notable attributes of low density and high specific strength. However, the low formability of Mg alloys at ambient temperature is a significant barrier to their widespread use. This is owing to hexagonal close-packed crystal structure of magnesium that offers only two slip systems for deformation at ambient temperature and resulting in low formability (Ref 1, 2). The strong basal texture observed in wrought magnesium alloys, which arises as a consequence of secondary deformation processes such as extrusion, rolling and sheet forming, gives rise to notable anisotropy in their mechanical properties, thereby

impacting their suitability for subsequent applications (Ref 3-6). When magnesium alloys are extruded, a strong final basal texture is produced with the grains aligned in the $\{0\ 0\ 0\ 1\}$ plane and $\langle 10\bar{1}0 \rangle$ direction parallel to the extrusion direction (Ref 3). For the basal slip, the deformation process in magnesium that is most readily triggered, these types of grain orientations are undesirable. When loads are applied parallel to the longitudinal axis of the extruded rod, the presence of strong basal texture further reduces the ductility of the material.

Extruded Mg alloys also demonstrate the tensile-compressive yield asymmetry. Specifically, the tensile yield strength is significantly greater than the compressive yield strength (Ref 7-10). The yield asymmetry is caused by the strong basal texture and is associated with twinning related issue. Twinning can support tensile strain along the c-axis in the hexagonal close-packed (HCP) crystal structure of magnesium (Mg), but not compressive strain. Twinning is the preferred deformation mechanism during the compression of extruded bars when the basal planes of the crystal structure align parallel to the direction of extrusion (Ref 11). Asymmetry can be reduced by deliberately suppressing the twinning process, which is possible by maintaining a fine average grain size in the extruded material. Apparently, twinning becomes more and more difficult when the grain size is reduced (Ref 3, 12). Grain coarsening is the result of high processing temperatures in extrusion process. The deformation of Mg alloys is only accomplished at the elevated temperatures since only two slip systems are available for the deformation at room temperature. The inclusion of second-phase particles in the morphology can

Ankush S. Marodkar and Hemant Borkar, Department of Metallurgical Engineering and Materials Science, Indian Institute of Technology Indore, Simrol, Indore, M. P. 453552, India; and Vivek Kumar Sahu, Department of Materials Science and Engineering, Indian Institute of Technology Kanpur, Kanpur, U.P. 208016, India; and School of Materials, The University of Manchester, Manchester M13 9PL, UK. Contact e-mail: h.borkar@iiti.ac.in.

limit grain coarsening during the secondary deformation process. Effective pinning sites for these boundaries can be provided by particles located near grain boundaries or those created by dynamic precipitation within the matrix during extrusion. As a result, they prevent the rapid increase in grain size in the extruded material (Ref 13, 14).

Alloying is the method used for refinement of grains, enhancement of mechanical properties and reducing yield asymmetry in wrought Mg alloys. Recently, it was demonstrated for wrought magnesium alloy that the individual or combined incorporation of rare earth elements (RE) enhances mechanical properties, weakens the texture and reduces the yield asymmetry. The improvement in mechanical properties and reduction in yield asymmetry have been attributed to $\{10\bar{1}2\}$ tensile-twin solid solution hardening and texture weakening (Ref 15-19). Bu et al. (Ref 20) studied the addition of Y and Gd in AZ80 alloy and found enhanced tensile and compression properties. In this case, the yield asymmetry was found to be reduced due to promotion of non-basal slip induced with the Gd, Y addition as well as particle-stimulated nucleation (PSN) mechanism induced by Y and Gd particles.

However, RE-free alloys are attractive because they are less expensive, yet only Ca has been shown to imitate the effects of RE texture weakening (Ref 21, 22). In the cast condition, Ca has demonstrated its effectiveness as a grain refiner in AZ81 alloy, up to a 1% addition. However, beyond this point, Ca induces grain coarsening. Moreover, the incorporation of 1% Ca leads to the enhancement of mechanical strength, with a subsequent decline observed beyond this threshold at room temperature (Ref 23). Li et al. (Ref 24) investigated the impact of adding 2, 4 and 6% Ca to AZ91 alloy following extrusion. Their findings indicate that a 2% Ca addition to AZ91 enhances its mechanical properties while surpassing this amount deteriorates the extruded AZ91-Ca alloy's performance. Allameh et al. (Ref 25) enhanced the mechanical properties of extruded AZ80-Ca by incorporating 0.5% Ca. Che (Ref 26) incorporated 1% Ca along with Re and Si into AZ91, resulting in improved mechanical properties at higher temperatures. These studies highlight the crucial role of Ca addition in enhancing the mechanical properties of extruded AZ series magnesium alloys. In addition to Ca, the other alkaline earth metal, Sr has proved to be the good candidate for reduction in average grain size along with reduction in yield asymmetry of the Mg alloys. Borkar et al. (Ref 27) studied the effect of Sr addition on Mg-Mn alloy. In his investigation, the Mg-Mn-Sr alloys demonstrated a weaker texture attributed to the emergence of randomly oriented texture components during the extrusion process. The occurrence of texture randomization during recrystallization is attributed to particle-stimulated nucleation (PSN) mechanism occurring at the interfaces of Mg-Sr intermetallic. In addition, M1-Sr compositions are discovered to have enhanced yield stress and % elongation as well as decreased yield asymmetry in his investigation. Similar results were obtained by Sadeghi et al. (Ref 28) with Sr addition in AZ31 alloy.

AZ91 is one of the most widely used commercial Mg alloys. Till date, there have been limited studies in the literature on individual Ca and Sr additions to cast or wrought AZ91 alloy and no studies on combined additions of Ca and Sr to wrought AZ91 alloy, specifically with regard to mechanical properties, texture and yield asymmetry. The principal aim of the current study is to produce high-strength extruded AZ91 with reduced tension-compression yield asymmetry by incorporating Ca and

Sr, thereby enhancing its suitability for structural applications. In this work, the AZ91-1Ca-xSr alloys were produced with squeeze casting technique and were further subjected to extrusion. The effect of combined alloying additions on microstructure, texture and mechanical properties including yield asymmetry was investigated. An in-depth characterization was also carried out to determine the recrystallization mechanisms responsible for texture weakening. Additionally, the findings from this study are compared with the existing literature on extruded commercial Mg-Al alloys.

2. Experimental Procedure

Casting of the alloys was carried out using the as-received AZ91 alloy and Mg-20 wt.% Ca and Mg-20 wt.% Sr master alloys. The SwamEquip's bottom pouring-type stir casting machine was used for casting of alloys. The melting was done by using bottom pouring stir casting electrical resistance furnace in the crucible under the inert gas atmosphere of Ar and SF₆. The melting setup was equipped with squeeze casting arrangement to obtain squeeze cast alloys. Blocks of AZ91 alloy underwent a melting process at a temperature of 700 °C, and appropriate amounts of Ca and Sr master alloys were introduced into the molten mixture. In order to ensure uniform distribution of the alloying elements, the melt was stirred up to 10 min. Following this, the melt was poured into the mild steel die having diameter 4 cm and length 30 cm and immediate squeezing was done at 100 MPa pressure for 30 s. The cylindrical cast rods were obtained for four targeted alloy compositions with 1 wt.% Ca and varying quantity of Sr (0.3-1.2 wt.%). The targeted and obtained alloy compositions using spark emission spectrometer along with alloy codes used in the present work are presented in Table 1. Thermodynamic analysis has been conducted using Thermo-Calc software and its TCMG6 database to simulate the formation of equilibrium phases.

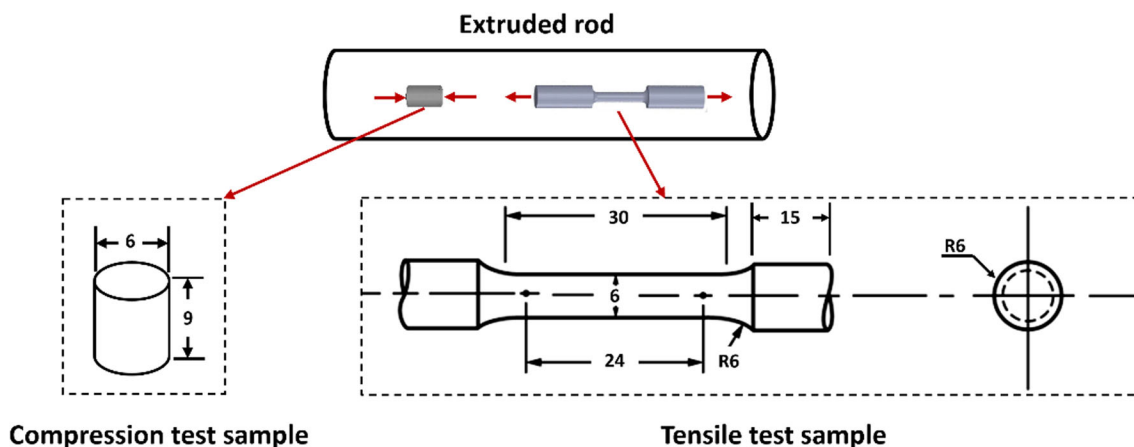
The machined squeeze cast billets with 4 cm diameter and 15 cm long were further subjected to hot extrusion process using SwamEquip's laboratory-scale 150-ton hydraulic press. The extrusions were carried out at 400 °C temperature and 1 mm/s initial ram speed with 4:1 extrusion ratio.

Bulk texture analysis was performed on the extruded rod cross section (perpendicular to extrusion direction) using Rigaku Ultima x-ray diffractometer with four circle goniometer in Schulz back-reflection geometry. Three incomplete pole figures ($0^\circ \leq \alpha \leq 70^\circ$) of $\{10\bar{1}0\}$, $\{0002\}$ and $\{10\bar{1}1\}$ poles were indexed with Cu-K_α radiation at the operating condition of 40 kV and 40 mA current. Further, bulk texture analysis was carried out by Resmat TexTools software for the orientation distribution function (ODF) calculation. ODFs were used to recalculate the inverse pole figures (IPF).

The extruded specimens underwent standard metallographic preparation, including polishing, followed by etching with an acetic picral solution composed of 2.5 gms of picric acid, 2.5 ml of acetic acid, 45 ml of ethanol and 5 ml of water for microstructure analysis. The optical microstructure was obtained using Zeiss axiovert a1 inverted microscope. JEOL JSM-7610 F plus field emission scanning electron microscope (FESEM) equipped with electron backscattered diffraction (EBSD) was used for microstructure and microtexture characterization. For EBSD analysis, the specimens were mechani-

Table 1 Targeted and obtained chemical compositions (wt.%) of extruded AZ91-1Ca-xSr Mg alloys

Alloy code	Targeted alloy composition	Obtained chemical composition, wt.%						
		Al	Zn	Mn	Si	Ca	Sr	Mg
E1	AZ91	9.02	1.56	0.18	0.021	Bal.
E2	AZ91-1 wt.% Ca-0.3 wt.% Sr	8.51	0.51	0.18	0.016	1.02	0.37	Bal.
E3	AZ91-1 wt.% Ca-0.6 wt.% Sr	8.22	0.49	0.18	0.015	1.11	0.74	Bal.
E4	AZ91-1 wt.% Ca-0.9 wt.% Sr	8.04	0.48	0.17	0.016	1.08	1.07	Bal.
E5	AZ91-1 wt.% Ca-1.2 wt.% Sr	7.98	0.47	0.18	0.017	1.12	1.41	Bal.

**Fig. 1** Geometry of compression and tensile test specimens (all dimensions are in mm)

cally polished with colloidal silica for 1 hr after final polishing with diamond suspensions (with $9 - 1 \mu\text{m}$) and the EBSD maps were generated using 20 kV accelerating voltage with $0.9 \mu\text{m}$ step size. Later, raw EBSD data were analyzed using HKL channel 5 system software.

The mechanical properties of the various compositions of extruded alloys were evaluated using uniaxial tensile and compression tests on a 100kN MTS-610 universal testing machine (UTM) at room temperature. Tensile tests were conducted on samples with gauge lengths of 24 mm and a diameter of 6 mm, initiating at strain rate of 0.001/s. Compression tests were performed on specimens of 6 mm in diameter and 9 mm in length at a constant strain rate of 0.001/s. The samples were cut from the center of the rod along extruded direction. Figure 1 shows the tensile and compression sample dimensions along with their locations in extruded rod.

3. Results

3.1 Bulk Texture

X-ray diffraction (XRD) analysis was used to identify the bulk textures in the extruded samples, and the resulting data is represented in the form of inverse pole figures (IPFs) in Fig. 2. All the alloys in the current study including base alloy AZ91 develop a fiber texture in which prismatic planes $\{10\bar{1}0\}$ are perpendicular to the extrusion direction. The maximum texture intensity of IPF represents the strength of the texture. It can be observed that the base alloy AZ91 produces a strong fiber texture featuring maximum texture intensity of 4.5 (Fig. 2a),

which further reduces to 4.1 with the incorporation of 1 wt.% Ca and 0.3 wt.% Sr (Fig. 2b). With an increase in Sr content from 0.3 to 0.9 wt.%, the texture intensity further weakens (Fig. 2c and d), demonstrating the effect of increased Sr content in extruded AZ91. The maximum texture intensity remains constant from 0.9 wt.% (Fig. 2d) to 1.2 wt.% Sr addition (Fig. 2e). Therefore, it can be deduced that the addition of Ca and Sr weakens the texture, and this effect is further pronounced with increasing Sr content in extruded AZ91 alloy.

An indirect approach was used to assess texture in extruded alloys in order to better understand the texture. The volume fraction of grains featuring basal planes in the radial direction may be equivalently expressed by the volume fraction of grains possessing prismatic planes perpendicular to the extrusion direction, owing to the development of basal fiber texture. This relationship has been previously discussed by one of the authors in this work, Borkar et al. (Ref 27). Also, the measurement of the volume fraction of the prismatic planes based on generated ODF from texture results is given in the literature by Sadeghi et al. (Ref 28). Figure 3 shows that volume fractions of prismatic planes for all extruded AZ91-1Ca-xSr alloys are less compared to extruded base AZ91 (E1 alloy), which exhibits the weakening of the fiber texture with combined Ca and Sr additions.

3.2 Thermodynamic Calculations

Figure 4 illustrates the outcomes of thermodynamic calculations predicting the equilibrium phases of all five alloys examined in the present study, based on their chemical compositions obtained from Table 1. In Fig. 4(a), the results indicate Mg and $\text{Mg}_{17}\text{Al}_{12}$ as major phases in AZ91, while

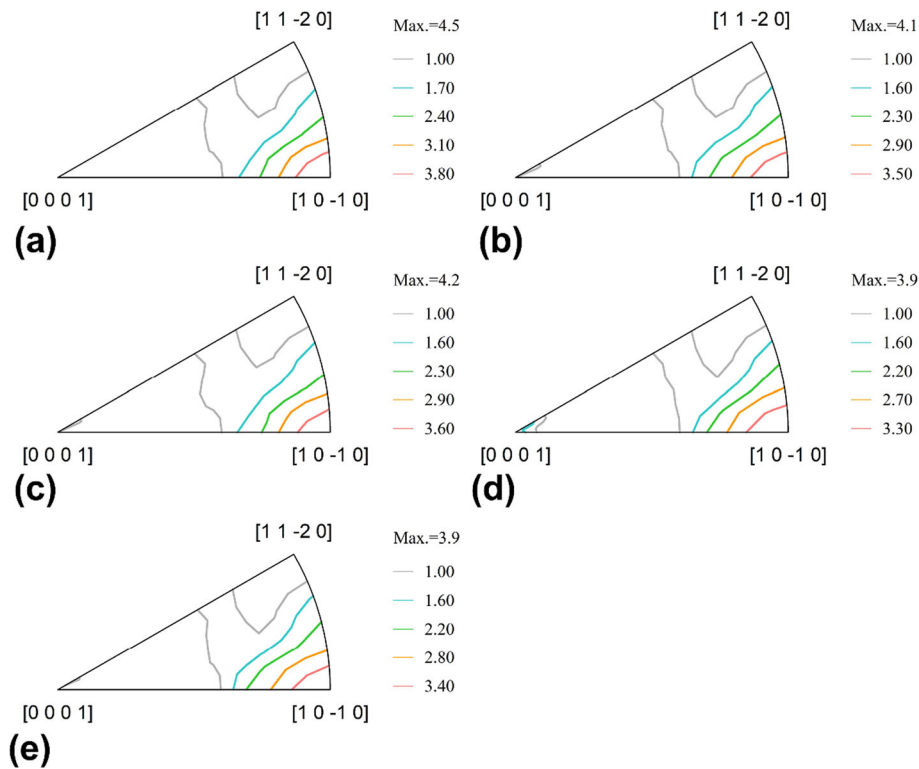


Fig. 2 Inverse pole figures (perpendicular to extrusion direction) of extruded samples: (a) E1 (AZ91), (b) E2 (AZ91-1Ca-0.3Sr), (c) E3 (AZ91-1Ca-0.6Sr), (d) E4 (AZ91-1Ca-0.9Sr), (e) E5 (AZ91-1Ca-1.2Sr)

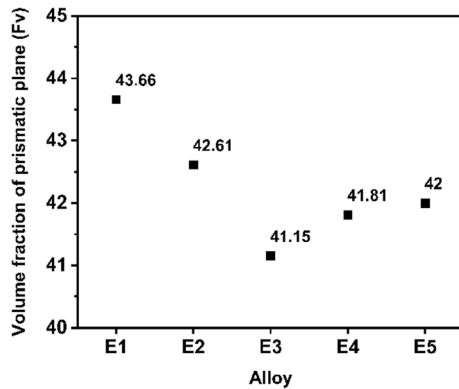


Fig. 3 Volume fraction of the prismatic planes having less than 20 degrees deviation from extrusion direction

other phases show Mg and Al intermetallic containing Mn and Si in very less quantities. During cooling, Mg matrix begins solidifying at 600 °C, whereas precipitation of $Mg_{17}Al_{12}$ starts at 355 °C. The addition of 1Ca-0.3Sr to AZ91 results in the evolution of Al_2Ca and Al_4Sr phases at 542.29 °C and 510.07 °C, respectively. For 1Ca-1.2Sr, a new $Mg_{17}Sr_2$ phase evolves after 500 °C. The volume fraction of $Mg_{17}Al_{12}$, Al_2Ca and Al_4Sr at room temperature and 400 °C (extrusion temperature in the present work) is tabulated in Table 2.

The calculated volume fraction of Al_2Ca is nearly consistent for all compositions at room temperature. Regarding the Al_4Sr phase, an increase in Sr content leads to an increment in the volume fraction at room temperature. A separate graph depicting the evolution of the Al_4Sr phase in all AZ91-1Ca-xSr alloys is presented in Fig. 5. It is observed that the volume

fraction of Al_2Ca and Al_4Sr slightly reduces at 400 °C compared to room temperature due to diffusion in the Mg matrix at high temperatures. However, both phases remain thermally stable even at 400 °C, which is the extrusion temperature for the present study.

Notably, with the addition of Ca and Sr, and subsequently with an increase in Sr content, the volume fraction of $Mg_{17}Al_{12}$ decreases. In contrast, that of Sr-containing precipitates increases at room temperature. Additionally, $Mg_{17}Al_{12}$ is not found at 400 °C. Therefore, from thermodynamic calculations, it can be predicted that $Mg_{17}Al_{12}$ does not participate in recrystallization during extrusion at 400 °C. Due to the thermal stability of Al_2Ca and Al_4Sr at 400 °C, it can be expected that these intermetallic phases primarily act as heterogeneous sites for nucleation and actively participate in recrystallization and texture weakening through particle-stimulated nucleation (PSN) during extrusion.

3.3 Microstructure of Extruded Alloys and Grain Size Measurement

Figure 6 presents the optical micrographs of all extruded AZ91-1Ca-xSr alloy samples with indication of extruded direction (ED). The microstructure analysis of extruded base AZ91 alloy sample (Fig. 6a) presents a bimodal morphology, featuring fine dynamically recrystallized (DRX) grains nucleated during extrusion and coarser deformed grains extended in the extrusion direction without recrystallization. With the addition of Ca and Sr to base AZ91 alloy, the microstructure consists of Al-Ca and Al-Sr stringers elongated in the extrusion direction as indicated in Fig. 6(b-e) for alloy samples E2 to E5. The microstructures of alloy E2 to E5 are seen to be fully recrystallized with some of the recrystallized grains around Al-

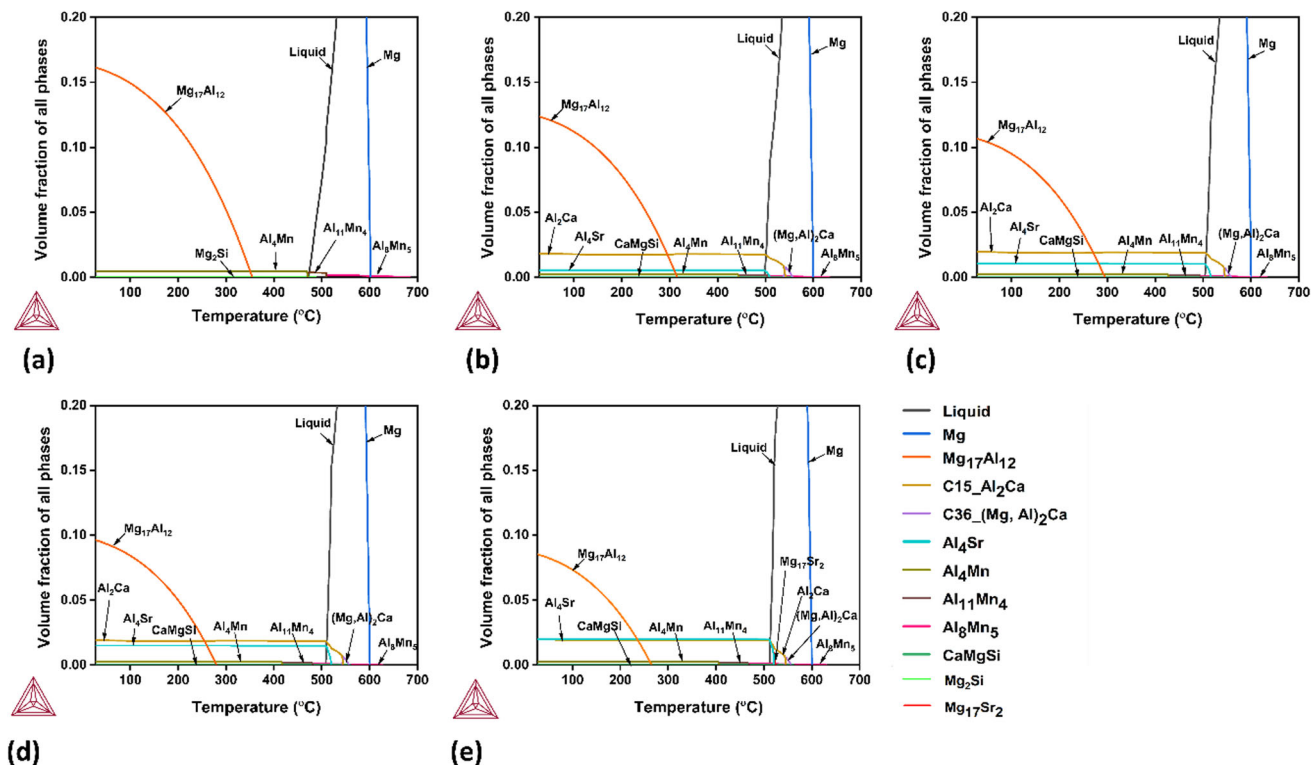


Fig. 4 Calculated equilibrium phases with different temperatures for (a) AZ91, (b) AZ91-1Ca-0.3r, (c) AZ91-1Ca-0.6Sr, (d) AZ91-1Ca-0.9Sr and (e) AZ91-1Ca-1.2Sr

Table 2 Volume fraction of $Mg_{17}Al_{12}$, Al_2Ca and Al_4Sr at room temperature and 400 °C obtained from Thermo-Calc prediction (in %)

Alloy	Phase					
	$Mg_{17}Al_{12}$		Al_2Ca		Al_4Sr	
	RT	400, °C	RT	400, °C	RT	400, °C
AZ91	16.141	0
AZ91-1 wt.% Ca-0.3 wt.% Sr	12.381	0	1.821	1.792	0.528	0.526
AZ91-1 wt.% Ca-0.6 wt.% Sr	10.682	0	1.962	1.931	1.045	1.040
AZ91-1 wt.% Ca-0.9 wt.% Sr	9.628	0	1.905	1.875	1.505	1.499
AZ91-1 wt.% Ca-1.2 wt.% Sr	8.538	0	1.972	1.942	1.984	1.975

Ca and Al-Sr stringers. With 1 wt.% Ca + 0.3 wt.% Sr and 1 wt.% Ca + 0.6 wt.% Sr additions to AZ91 (E2 and E3 alloy), the discontinuous network of stringers is obtained, whereas, with 1 wt.% Ca + 0.9 wt.% Sr and 1 wt.% Ca + 1.2 wt.% Sr additions (E4 and E5 alloy), homogeneous and continuous network of stringers is obtained. The incorporation of Ca and Sr to extruded base AZ91 alloy leads to grain size reduction, which has been later confirmed with EBSD analysis in this manuscript.

Dynamic recrystallization (DRX) mechanisms in magnesium alloys can be broadly divided into continuous DRX (CDRX), twin-induced DRX (TDRX) and discontinuous DRX (DDRX) (Ref 29, 30). In brief, CDRX and TDRX are prominent mechanisms at temperatures lower than 300 °C; conversely, DDRX takes precedence at temperatures above this threshold. (Ref 31). High deformation temperature in the DDRX process results in a little change in the critical resolved

shear stress (CRSS) for basal slip but a large drop in the CRSS for other slip systems, reducing the difference between the two (Ref 32). Consequently, the engagement of an enough number of slip systems to introduce plastic deformation results from the initiation of non-basal slip at elevated temperatures (400 °C in the present work) and hinders the initiation of twin formation. As a result, in the present work, extrusion at 400 °C suppresses the development of twins, and therefore, twins are not found in the optical micrographs of extruded AZ91 and AZ91-1Ca-xSr alloys (Fig. 6), and as dislocation slip takes precedence, it facilitates the expansion of grain boundaries into areas characterized by high dislocation densities. The phenomenon of grain boundary migration, which unfolds during subsequent deformation, progressively augments the misorientation between the parent grain and the bulging subgrain, resulting in the generation of a new strain-free grain. The extruded AZ91-1Ca-xSr alloy contains a significant fraction of DRXed grains, and

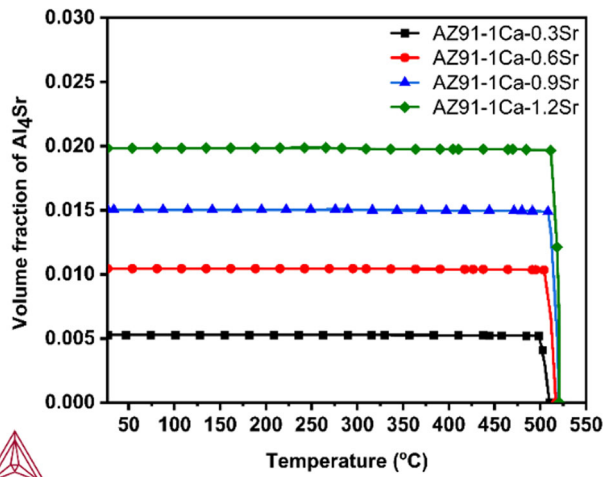


Fig. 5 Calculated volume fraction of Al₄Sr in AZ91-1Ca-xSr alloys

the unDRXed grains in the alloy have a relatively equiaxed morphology. Here, due to the presence of stringers in extruded AZ91-1Ca-xSr alloys, along with grain boundary bulging, particle-stimulated nucleation (PSN) is a probable mechanism for the formation of recrystallized grains around the stringers.

Figure 7 shows the FESEM micrographs of all extruded alloys, along with EDS spectrums of Al-Ca and Al-Sr precipitates. It is observed from the AZ91 micrograph in Fig. 7(a) that the β -phase network is broken into tiny precipitates which are distributed throughout the microstructure. In contrast, AZ91-1Ca-xSr alloys contain the stringer-like structure of secondary precipitates. The well-developed network of stringers can be observed when Sr levels are increased from 0.3 wt.% (alloy E2) to 1.2 wt.% (alloy E5) (Fig. 7b-e). FESEM micrograph findings exhibit congruence with the outcomes derived from optical micrographs (Fig. 6). With the incorporation of Ca and Sr in the base alloy AZ91 up to the levels added in the present work, the Al₂Ca and Al₄Sr

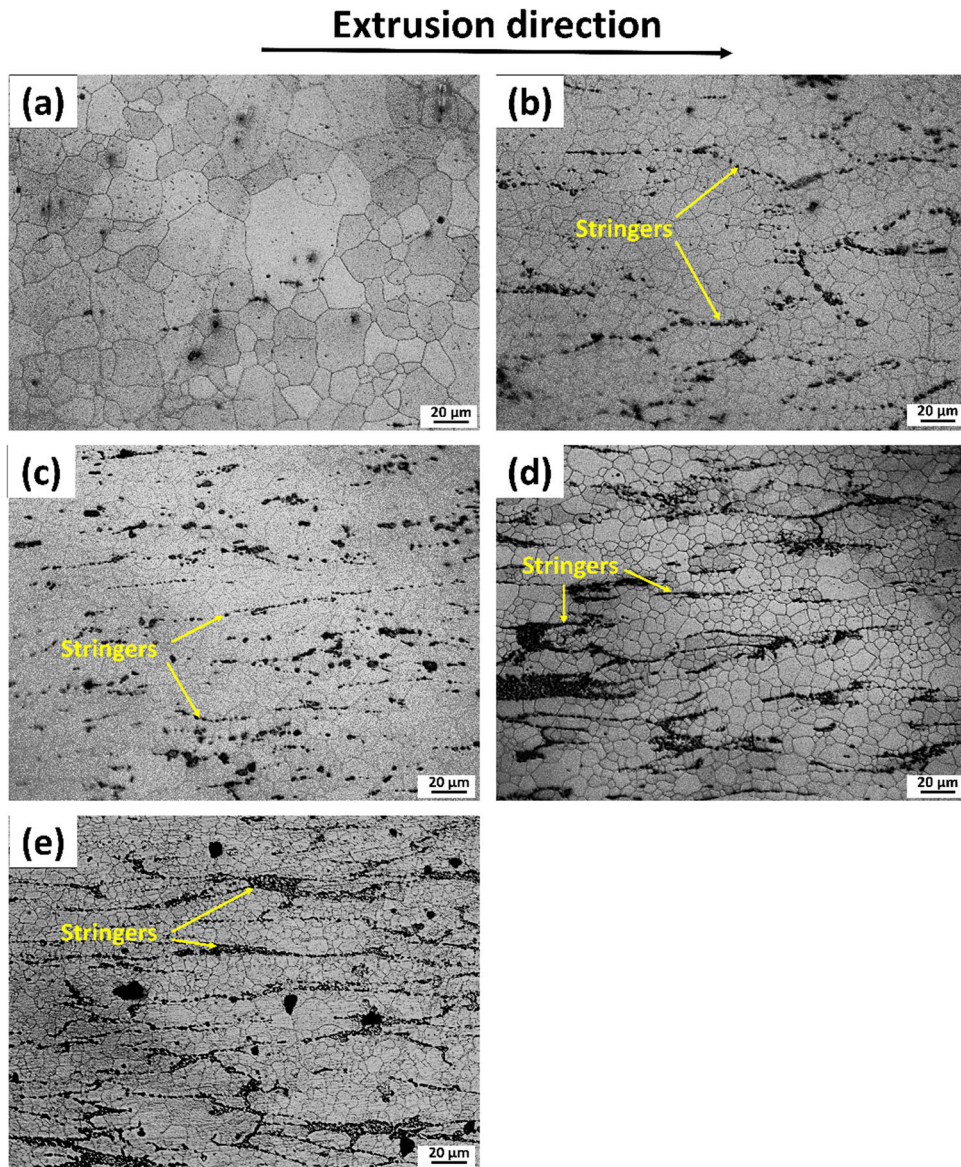


Fig. 6 Optical micrographs of extruded samples (extrusion direction as indicated): (a) E1 (AZ91), (b) E2 (AZ91-1Ca-0.3Sr), (c) E3 (AZ91-1Ca-0.6Sr), (d) E4 (AZ91-1Ca-0.9Sr), (e) E5 (AZ91-1Ca-1.2Sr)

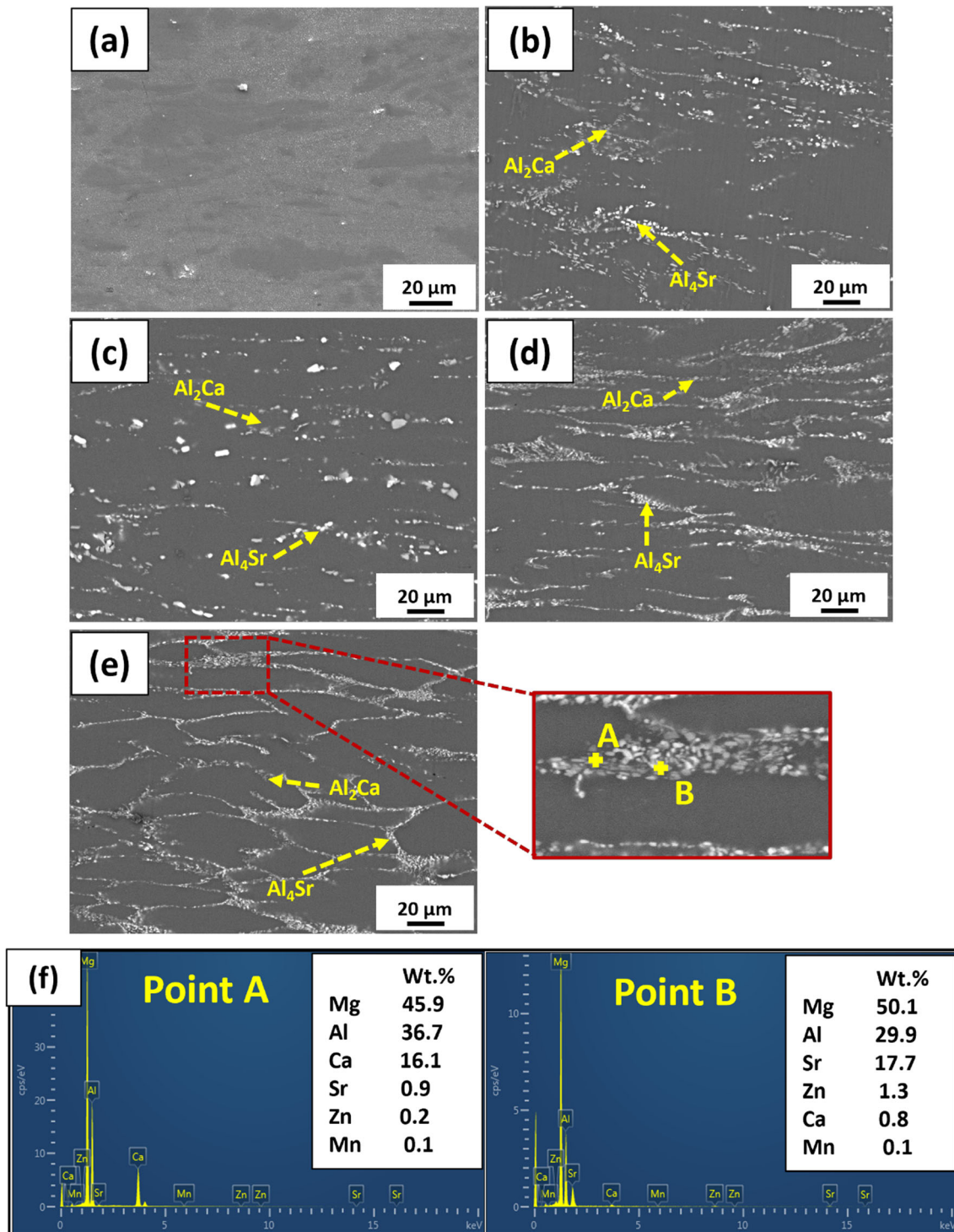


Fig. 7 FESEM micrographs of extruded samples in BSE mode (extrusion direction is horizontal): (a) E1 (AZ91), (b) E2 (AZ91-1Ca-0.3Sr), (c) E3 (AZ91-1Ca-0.6Sr), (d) E4 (AZ91-1Ca-0.9Sr), (e) E5 (AZ91-1Ca-1.2Sr); (f) EDS spectrum of marked points in the magnified image of rectangular section in the E5 alloy (AZ91-1Ca-1.2Sr) micrograph

precipitates are formed and can be identified depending on the atomic number of the elements they contain in the FESEM images in BSE mode as shown in Fig. 7. As a result of the greater atomic number of strontium (38) in comparison with other elements, the Al_4Sr intermetallic displays a more luminous appearance as compared to Al_2Ca . Figure 7(f) shows the EDS spectrum, confirming the more luminous Al-Sr

precipitates and the less luminous Al-Ca precipitates. The formation of these precipitates has been discussed in our previous work on Ca and Sr addition in squeeze cast AZ91 alloy (Ref 33). The incorporation of Ca and Sr into the squeeze cast AZ91 alloy led to the development of a continuous and finer secondary interdendritic network. Additionally, this process led to the emergence of lamellar Al_2Ca and Al_4Sr phases,

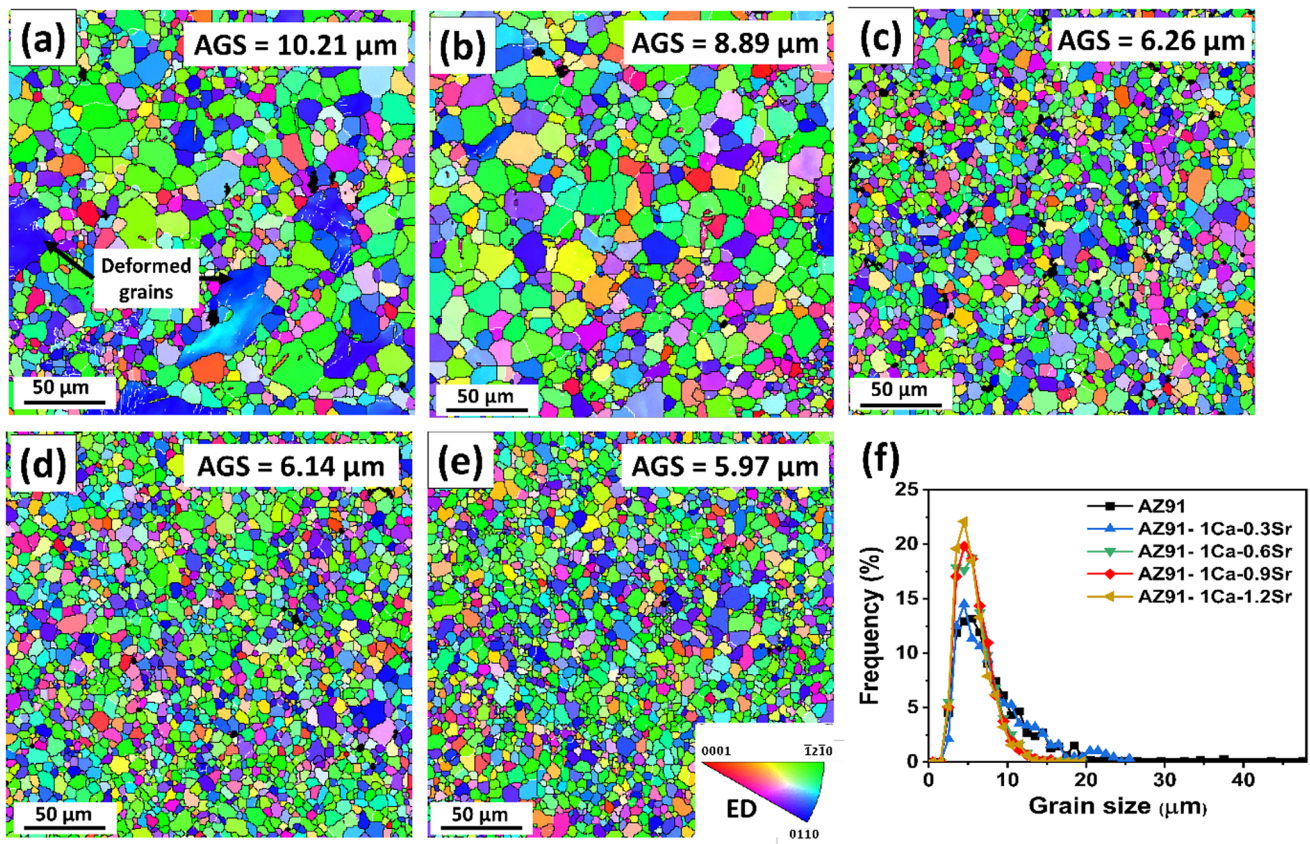


Fig. 8 IPF maps along with the grain size distribution maps for extruded (a) E1 (AZ91), (b) E2 (AZ91-1Ca-0.3Sr), (c) E3 (AZ91-1Ca-0.6Sr), (d) E4 (AZ91-1Ca-0.9Sr), (e) E5 (AZ91-1Ca-1.2Sr) (all maps are plotted perpendicular to the extrusion direction), (f) grain size distribution graph

while simultaneously suppressing the existence of the β -Mg₁₇Al₁₂ phase (Ref 33). The Al₂Ca and Al₄Sr are thermally stable precipitates with high melting points compared to β -Mg₁₇Al₁₂ precipitates (Ref 33, 34). Therefore, at an extrusion temperature of 400 °C, thermally stable Al₂Ca and Al₄Sr precipitates are fragmented in the form of discontinuous stringers and are extended in the direction of extrusion (Fig. 7). The thermal stability of Al₂Ca and Al₄Sr precipitates at 400 °C is also predicted by thermodynamic calculations in section 3.2 in the present work.

The grain size of extruded alloys was determined through EBSD analysis. EBSD scans were obtained for all the extruded alloys, and their inverse pole figure (IPF) maps along with their grain size distribution maps are illustrated in Fig. 8. The initial obtained grain size of the squeeze cast AZ91 alloy is 63.02 μ m (Ref 33), and after extrusion, the average grain size is reduced to 10.21 μ m (Fig. 8a). With the initial addition of Ca and Sr in alloy E2 (Fig. 8b), the grain size is reduced to 8.89 μ m, and the distribution range of the grain diameter narrows (Fig. 8f). With an increase in Sr content, the average grain size is further reduced, showing a more homogeneous grain size distribution compared to the base alloy AZ91. The E2, E3, E4 and E5 alloys show 12.93, 38.68, 39.86 and 41.52% reduction in average grain size compared to the base alloy AZ91 (E1), respectively. Figure 9 illustrates the relationship between the increase in Sr content and the corresponding reduction in grain size. Feng Li et al. (Ref 24) and Guan Shao-kang et al. (Ref 35) made similar observations about the effect of calcium (Ca) addition in extruded AZ91 alloy and strontium (Sr) addition in extruded

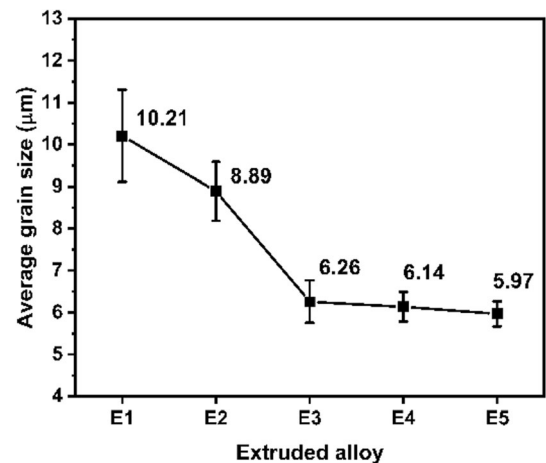


Fig. 9 Average grain size plot measured from IPF maps of extruded alloys

AZ80 alloy, respectively. Here, the reduction in the grain size of extruded AZ91-1Ca-xSr alloys, compared to the base alloy, is attributed to the grain boundary pinning mechanism resulting from secondary Al₂Ca and Al₄Sr phases. With increasing Sr levels, the quantity of Al₄Sr increases, enhancing the grain boundary pinning effect and leading to a further reduction in grain size.

Figure 10 presents the image quality (IQ) map along with IPF map of extruded AZ91 (base E1 alloy) and AZ91-1Ca-

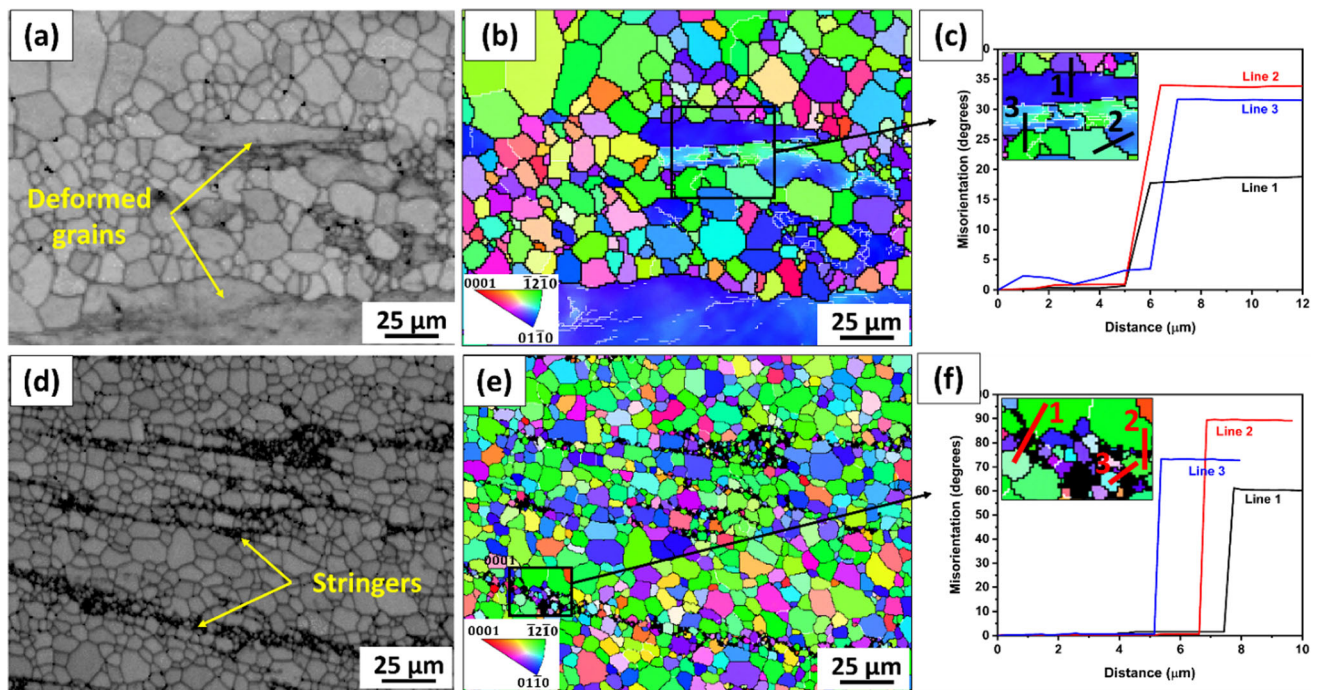


Fig. 10 Electron backscattered diffraction (EBSD) microstructure: (a) IQ map, (b) inverse pole figure map, (c) point-to-origin misorientation line profile graph of extruded AZ91 and (d) IQ map, (e) inverse pole figure map, (f) point-to-origin misorientation line profile graph of extruded AZ91-1Ca-1.2Sr (extrusion direction is horizontal and all maps use IPF colors referring to the extrusion direction)

1.2Sr (E5 alloy). Considering IQ and IPF maps, the three types of grains can be identified, viz. deformed grains (mainly in base alloy AZ91), larger-sized recrystallized grains and small-sized recrystallized grains. The progressive shift in color in the deformed grains suggests localized strain and the existence of low-angle grain boundaries. Typically, grains displaying low-angle grain boundaries alongside an internal misorientation spread exceeding 2° are categorized as parent grains exhibiting deformation. The color variation within these grains serves as an indicator of localized deformation. Meanwhile, recrystallized grains are distinguished by their uniform coloration and an internal misorientation spread of less than 2° . White-colored grain boundaries correspond to low-angle boundaries, whereas black-colored grain boundaries signify high-angle boundaries. In the AZ91-1Ca-1.2Sr alloy, the Al_2Ca and Al_4Sr stringers are elongated in the extruded direction (Fig. 6 and 7) and form a neckless-type structure. The EBSD orientation map portrays the stringers with a representation in black color. Recrystallized grains are observed within the matrix and surrounding the stringers within the microstructure. Distinct categorization of these recrystallized grains is achievable based on their proximity to the stringers.

Particle-stimulated nucleation (PSN) is a probable mechanism for the formation of recrystallized grains around the stringers in AZ91-1Ca-1.2Sr alloy. There are recrystallized grains around parent deformed grains observed in the microstructure of extruded base AZ91 alloy as well as in AZ91-1Ca-1.2Sr alloys (not associated with stringers) which are most probably formed by grain boundary bulging mechanism, a type of DDRX mechanism. Extruded AZ91-1Ca-1.2Sr exhibits the reduction in average grain size compared to that of base alloy and with the presence of extensive network of stringers (Fig. 6 and 7), and PSN is the crucial recrystallization

mechanism that decides the final texture in this alloy. PSN is also expected to affect the final texture in all alloys E2 to E5 with Ca and Sr additions in this study, and the fraction of grains recrystallized by PSN is expected to increase with increasing Sr addition to AZ91.

To study the grain boundary bulging and PSN in detail, the misorientation degrees are calculated for the recrystallized grains associated with parent deformed grains (in AZ91 alloy) and recrystallized grains associated with stringers (in AZ91-1Ca-1.2Sr alloy) in Fig. 10(c) and (f), respectively. It is noteworthy that when the recrystallized grains surrounding the stringers collided with another grain or stringer, their growth stopped. Figure 10(c) presents the inset of Fig. 10(b) indicating the misorientation between the deformed grain and three recrystallized grains associated with the deformed grains. The misorientation profile plotted across the deformed grain and grain associated with deformed grain (line 1, 2 and 3 in Fig. 10c) shows the characteristic misorientation of 15° to 35° , whereas the misorientation profile plotted across the two grains separated by the stringers (line 1, 2 and 3 in Fig. 10f) shows the characteristic misorientation of 55° to 90° . In Fig. 10(c), the recrystallized grains that have originated from parent deformed grains (for AZ91 alloy) are likely a result of the grain boundary bulging mechanism, as evidenced by their relatively smaller difference in misorientation with those of parent deformed grains. In contrast, the recrystallized grains that originated from stringers in AZ91-1Ca-1.2Sr alloy (Fig. 10f) have wider difference in misorientation with each other, which is a characteristic of PSN mechanism produced by second-phase particles in the microstructure. In this study, PSN is most likely generated by intermetallic particles of Al_2Ca and Al_4Sr present in the form of elongated stringers parallel to extrusion direction which causes texture weakening in the AZ91 alloy.

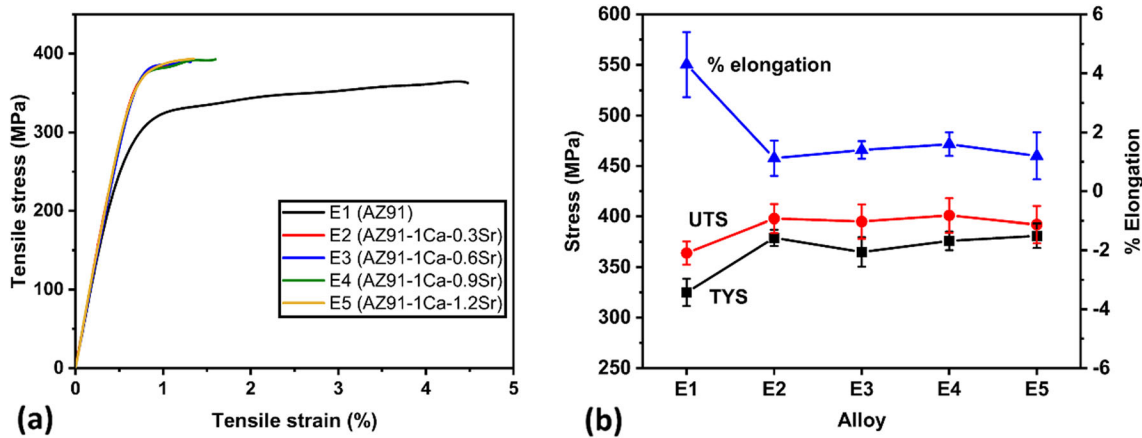


Fig. 11 (a) Engineering stress strain curve and (b) its respective values of tensile yield stress (TYS), ultimate tensile stress (UTS) and % elongation for tensile test of extruded alloys at room temperature

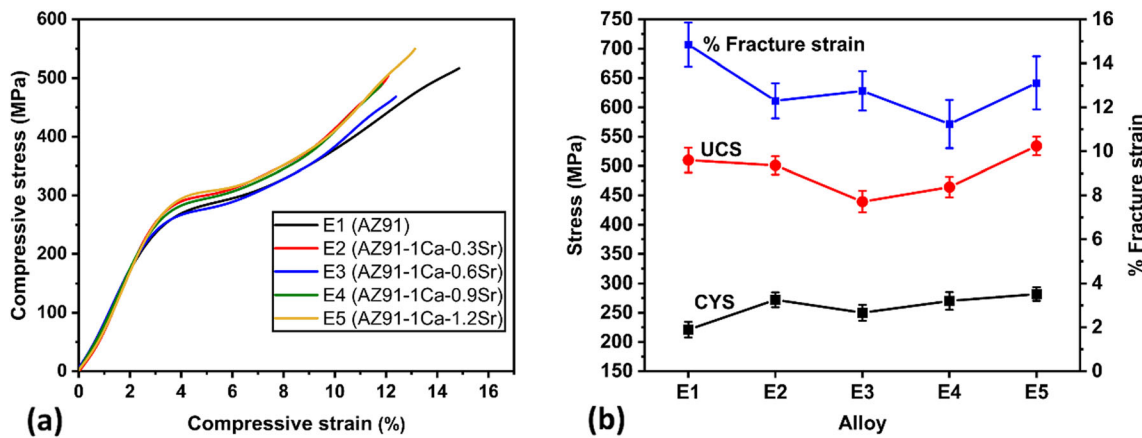


Fig. 12 (a) Engineering stress strain curve and (b) its respective values of compressive yield stress (CYS), ultimate compressive stress (UCS) and % fracture strain for compression test of extruded alloys at room temperature

3.4 Mechanical Properties

The tensile and compressive properties of extruded alloys are plotted in Fig. 11 and 12, respectively, while the numerical values of these properties are presented in Tables 3 and 4, respectively.

Figure 11 and Table 3 show that both the tensile yield strength (TYS) and ultimate tensile strength (UTS) increase upon the initial incorporation of Ca and Sr (1wt.% Ca-0.3wt.% Sr) to AZ91 alloy. This trend of enhanced tensile strength holds consistent across all extruded AZ91-1Ca-xSr alloys. However, a reduction in % elongation (%El) is observed across all AZ91-1Ca-xSr alloys, exhibiting irregular behavior. E4 alloy (extruded AZ91-1wt.% Ca-0.9 wt.% Sr) shows the good combination of all three tensile properties (TYS, UTS and % El). Specifically, compared to the base AZ91 alloy, the TYS and UTS in the E4 alloy exhibits increases of 15.7% and 10.2%, respectively, while the % El shows a significant reduction of 62.8%. Furthermore, as the Sr content is gradually increased to 1.2%, elongation and UTS degrade.

Figure 12 and Table 4 reveal that the CYS increases with the addition of Ca and Sr to AZ91, whereas the UCS and % fracture strain show irregular behavior. The highest CYS and

UCS values are obtained with 1wt.% Ca + 1.2wt.% Sr additions (in E5 alloy). The % fracture strain reduces with the addition of Ca + Sr for all studied compositions compared to base AZ91. The E5 alloy exhibit the balanced combinations of all three compressive properties, with improvement of 27.6% and 4.7% in CYS and UCS, respectively, compared to the base AZ91 (E1 alloy).

It is evident that the difference between TYS and UTS is smaller (Fig. 11) compared to the difference between CYS and UCS (Fig. 14). Being the measure of strain hardening, the difference in yield stress and fracture stress in both tensile and compression graphs shows that the strain hardening is higher in the compression than tension for the extruded AZ91-1Ca-xSr alloys. Furthermore, fracture strain (%) is much greater under compression compared to tension.

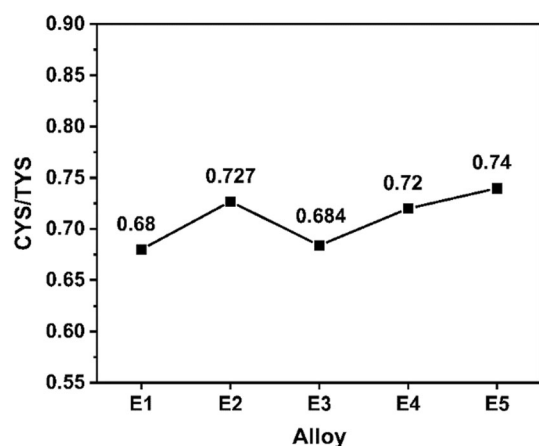
Figure 13 presents the yield asymmetry (CYS/TYS) for all five extruded alloys and the graph is plotted based on the values obtained from tensile and compressive testing. It can be observed that the CYS/TYS is increasing with combined Ca and Sr additions for all alloys (i.e., yield asymmetry is reducing). The highest CYS/TYS value is obtained for the extruded AZ91-1%Ca-1.2%Sr alloy (E5 alloy).

Table 3 Tensile properties of extruded alloys

Code	Composition	TYS, MPa	UTS, MPa	Elongation, %
E1	AZ91	325 ± 13.5	364 ± 11.4	4.3 ± 1.1
E2	AZ91-1 wt.% Ca-0.3 wt.% Sr	379 ± 8.1	398 ± 14.2	1.12 ± 0.6
E3	AZ91-1 wt.% Ca-0.6 wt.% Sr	365 ± 14.6	395 ± 16.9	1.4 ± 0.3
E4	AZ91-1 wt.% Ca-0.9 wt.% Sr	376 ± 9.2	401 ± 17.0	1.6 ± 0.4
E5	AZ91-1 wt.% Ca-1.2 wt.% Sr	381 ± 12.1	392 ± 18.3	1.2 ± 0.8

Table 4 Compressive properties of extruded alloys

Code	Composition	CYS, MPa	UCS, MPa	Fracture strain, %
E1	AZ91	221 ± 13.2	510 ± 21.3	14.85 ± 1.0
E2	AZ91-1 wt.% Ca-0.3 wt.% Sr	272 ± 12.6	501 ± 15.6	12.3 ± 0.8
E3	AZ91-1 wt.% Ca-0.6 wt.% Sr	250 ± 13.8	439 ± 18.4	12.75 ± 0.9
E4	AZ91-1 wt.% Ca-0.9 wt.% Sr	270 ± 15.1	464 ± 17.5	11.24 ± 1.1
E5	AZ91-1 wt.% Ca-1.2 wt.% Sr	282 ± 11.6	534 ± 16.0	13.11 ± 1.2

**Fig. 13** Yield asymmetry plot (CYS/TYS) for extruded alloys

4. Discussion

4.1 Microstructure and Texture Development

The final microstructure and texture development of the extruded alloys in this work are determined by recrystallization mechanisms taking place during and after deformation. The recrystallization mechanisms are influenced by the composition of the alloy while temperature and strain rate of the extrusion process also have an impact. The extruded microstructure is characterized by grain size and the nature of second phases present which also impact the recrystallization mechanisms and the overall texture that is developed after extrusion.

The AZ91 base alloy exhibits a typical magnesium texture following extrusion, primarily due to the occurrence of preferential basal slip during the extrusion process. At 400 °C, the CRSS for non-basal slip systems reduces and comes closer to the CRSS of basal slip systems. Hence, a significant number of slip systems are initiated to introduce plastic deformation and thus obstruct the formation of deformation twinning. The reduction in texture intensity can be

observed in all extruded AZ91-1Ca-xSr alloys (E2 to E5) with increase in Sr content compared to extruded AZ91. This shows that the basal texture is weakened with incorporation of Ca and Sr to base AZ91 alloy.

In AZ91-Ca-xSr extrusions, the presence of Al₂Ca and Al₄Sr precipitates serves as initiation points for the PSN phenomenon by creating localized variations in strain energy. PSN, in turn, produces grains with random orientations, thus diminishing the overall sharpness of the texture. The base AZ91 alloy mainly shows the recrystallization based on grain boundary bulging. The AZ91-1Ca-xSr alloys with 0.9 wt.% and 1.2 wt.% Sr show lower texture intensity compared to other alloys due to higher propensity of PSN with higher second-phase fraction available for PSN in these compositions. Ca and Sr additions to AZ91 alloy also result in grain refinement of the microstructure since both of these alloying elements have demonstrated their effectiveness as grain refiners for Mg alloys in past studies as well (Ref 24, 25, 27, 28).

4.2 Effect of Ca and Sr Additions on Mechanical Properties

The mechanical behavior of extruded Mg alloys is influenced by different strengthening mechanisms mainly solid solution hardening, grain boundary hardening and precipitate hardening. In the extruded AZ91-1Ca-xSr alloys, the solubility of Ca and Sr in the α -Mg matrix is limited, i.e., solubility of Ca in Mg is 0.05 at.% and Sr in Mg is 0.04 at.% (Ref 36, 37). Hence, within all AZ91-1Ca-xSr alloys, only a minimal portion of calcium (Ca) and strontium (Sr) persists in the form of solute atoms within the α -Mg matrix of the extruded AZ91. Consequently, while the presence of dissolved Ca and Sr in the AZ91 alloys does indeed invoke a solid solution hardening effect, its impact remains relatively modest due to the constrained quantity of dissolved calcium and strontium. Hence, Ca and Sr consume Al from Mg₁₇Al₁₂ and form Al₂Ca and Al₄Sr precipitates (Ref 33). Due to their high melting points, they remain stable at the extrusion temperature (400 °C) and form stringer-like structure. With 1.2% Sr additions, the dense neckless structure of the stringers can be observed (Fig. 6 and 7). The precipitates of Al₂Ca and Al₄Sr act as the barriers to the

dislocation glide and provide the precipitation strengthening effect which further results in enhancement of mechanical properties. Another important aspect of improved mechanical properties of AZ91-1Ca-xSr alloys is the change in the microstructure, i.e., increase in grain boundary density. The grain size reduction with Ca and Sr addition leads to the improvement in mechanical properties of extruded alloys. The addition of 1 wt.% Ca and 0.3 wt.% Sr (in E2 alloy) leads to a significant reduction in grain size compared to extruded base alloy AZ91 (E1). However, subsequent additions of Sr do not lead to a substantial alteration in grain size. A similar trend is also evident in the mechanical properties in tensile and compression testing. With 1% Ca and 0.3% Sr additions (E2), the TYS is improved by 16.62% compared to base AZ91 alloy (E1), whereas the further increase in Sr from 0.3 to 1.2% (E5) leads to only 0.52% improvement in TYS. Similarly, in the compressive testing, the E2 alloy shows 23.07% enhanced CYS compared to E1, whereas E5 showed only 3.7% enhancement in CYS from E2 to E5 alloy.

The intensities of both grain boundary hardening and precipitate hardening exhibit a noticeable rise as the strontium (Sr) content increases. This phenomenon is attributed to reduced average grain size and the rise in the presence of precipitates associated with higher Sr content. As all extruded AZ91-1Ca-xSr alloys feature a fully dynamically recrystallized (DRXed) grain structure, the average grain size in these alloys is primarily influenced by the rate of grain growth of the newly formed DRXed grains. The increase in the quantity of precipitates contributes to an augmented degree of grain boundary pinning, subsequently enhancing the PSN mechanism. This, in turn, results to the formation of smaller DRXed grains and a subsequent reduction in the average grain size.

For temperatures below 350 °C, CDRX and TDRX are the dominant mechanisms for deformation, while DDRX becomes dominant above this temperature. At lower temperatures, texture weakening occurs due to the formation of a necklace structure of fine grains attributed to CDRX and the simultaneous formation of new DRXed grains at the twin boundaries through the TDRX mechanism. However, in the present work, at 400 °C, a network of fine grains is not observed, as CDRX and TDRX are not feasible at this temperature. In comparison, extrusion at higher temperatures exhibits a stronger texture compared to temperatures below 350 °C. Furthermore, an increase in extrusion temperature results in larger grain sizes for both DRXed and unDRXed grains, reducing TYS and CYS values. Therefore, at higher temperatures, PSN plays a major role in strength enhancement and texture weakening since CDRX and TDRX mechanisms are not applicable (Ref 38, 39).

In this study, the initial AZ91 extruded alloy displays a pronounced basal texture, characterized by the alignment of the majority of the basal planes in parallel with the extrusion direction. Consequently, the AZ91 alloy, with its larger grain size, demonstrates the lowest yield strength (TYS). In cases where a material displays a preferred orientation, the yield asymmetry (CYS/TYS) becomes more pronounced. This is because most magnesium (Mg) alloys tend to undergo twinning along the c-axis of the hexagonal close-packed (HCP) unit cell during tensile loading. The basal texture identified in the AZ91 alloy encourages twinning to occur during compression rather than in tension, particularly in alignment with the extrusion direction. Consequently, AZ91 alloy exhibits the highest yield asymmetry, with a CYS/TYS ratio of 0.68. Additionally, the AZ91 alloy, distinguished by its comparatively larger grain

size, exhibits the highest fracture strain under compression, thus indicating a significant contribution of twinning to the deformation behavior within this alloy. The incorporation of Ca and Sr elements reduces the yield asymmetry of extruded AZ91 alloy by introducing randomness to the texture and decreasing the grain size. With increasing Sr content, the values of stress parameters such as tensile yield strength (TYS), ultimate tensile strength (UTS) and compressive yield strength (CYS) gradually increase. This phenomenon is attributed to the process of precipitate hardening caused by the presence of Ca and Sr. Hence, the variations in mechanical properties observed in different AZ91-1Ca-xSr alloys in the present work are primarily determined by their texture and hardening behavior.

4.3 Comparison of Tensile and Compressive Properties of Extruded AZ91-Ca-Sr Alloy with Developed Extruded AZ Series Mg Alloys

Table 5 presents the values of tensile properties of the extruded AZ series Mg alloys in the available literature and shows its comparison with the present work. For better clarity, Fig. 14 depicts a UTS versus elongation graph, incorporating the optimized combinations of our developed alloy and those reported in the literature. The prepared extruded AZ91 alloy in the present work showed superior tensile strength with reasonable percentage elongation compared to previously developed extruded AZ91 without alloy additions. Considering E4 alloy (AZ91-1 wt.% Ca-0.9 wt.% Sr), which showed the highest tensile strength in the present work, also exhibits superior tensile strength compared to almost all developed extruded AZ91 with alloy additions (Ca, Sr, Mn, Sn, Si, REs, etc.) except Mg-xAl-3Ca-0.3Mn alloys ($x = 5, 6, 7$).

Table 6 presents the values of compressive properties of the AZ series Mg alloy in the available literature and shows its comparison with present work. Figure 15 illustrates the UCS versus fracture strain, incorporating optimized combinations of developed alloy in the present work and alloys reported in the literature. The prepared extruded AZ91 alloy in the present work showed all three enhanced compressive properties compared to previously developed extruded AZ91 without alloy additions. Also, the E5 alloy (AZ91-1 wt.% Ca-1.2 wt.% Sr) showed the highest compressive strength with good fracture strain, standing at a very good position among all developed extruded AZ91 with alloy additions. Hence, extruded AZ91-1Ca-xSr alloy developed in the present work are the promising candidates for the structural applications considering developed extruded AZ series Mg alloys.

5. Conclusion

In the present work, the AZ91-1Ca-xSr alloys with different compositions were produced with squeeze casting technique followed by hot extrusion. The effect of combined Ca and Sr additions on microstructure, texture and mechanical properties in extruded AZ91-1Ca-xSr alloys was studied. The prevailing recrystallization mechanisms and the role of second phases in the deformation behavior were also subjected to detailed characterization. The conclusions from the study are summarized below:

Table 5 Tensile properties comparison with the available literature

Alloy	Extrusion parameters			Tensile Properties			References
	Ram speed, mm/s	Temp., °C	Extrusion ratio	TYS, MPa	UTS, MPa	El, %	
AZ91	...	300	36:1	251	361	10.7	(Ref 40)
AZ91		340	25:1	258 ± 5	439 ± 1	15.5 ± 0.3	(Ref 41)
AZ91	8	300	5.5:1	...	327	4.5	(Ref 42)
		360		...	321	8.9	
		300	22:1	...	307	13.7	
		360		...	295	13	
AZ91	...	400	22:1	...	~ 340	~ 10.2	(Ref 24)
AZ91-2Ca				...	~ 342	~ 9.5	
AZ91-4Ca				...	~ 335	~ 5.8	
AZ91-8Ca				...	~ 330	~ 5.9	
AZ91-2Ca-0.2Mn	0.084	250	44:1	271	364	8.9	(Ref 43)
		275		260	362	10.3	
		300		215	328	12.1	
		350		208	316	12.2	
		400		227	319	7.8	
AZ80	20	330	12:1	...	306	12.2	(Ref 44)
AZ80	1	250	8:1	241 ± 17	323 ± 12	5.5 ± 0.1	(Ref 39)
		300		210 ± 2	310 ± 6	6.2 ± 0.7	
		350		194 ± 5	327 ± 3	13.1 ± 0.5	
AZ80	10	280	12:1	...	304 ± 7	12 ± 2	(Ref 25)
AZ80-0.1Ca				...	320 ± 4	15 ± 3	
AZ80-0.5Ca				...	329 ± 3	19 ± 5	
AZ80		340		...	305 ± 6	11 ± 4	
AZ80-0.1Ca				...	311 ± 3	12 ± 5	
AZ80-0.5Ca				...	312 ± 2	8 ± 3	
AZ80	...	395 ± 5	3.6 :1	...	312	8	(Ref 35)
AZ80 + 0.02Sr				...	320	9.6	
AZ80 + 0.16Sr				...	310	12.5	
AZ80 + 0.30Sr				...	308	13.3	
AZ91-0.9RE-0.1Sr	...	420	12:1	234.00	335.13	21.11	(Ref 45)
AZ91-1Ca-0.5Si-0.1La-0.1Ce	1.45	360	30:1	278	318	9.2	(Ref 26)
Mg-8Al-0.5Zn-0.2Mn-0.3Ca-0.2Y	1	250	8:1	307 ± 9	398 ± 16	5.8 ± 1.2	(Ref 46)
		350		194 ± 7	327 ± 1	13.8 ± 1.9	
Mg-3.6Al-3.3Ca-0.4Mn	0.1	350	20:1	410	420	~ 6.3	(Ref 47)
Mg-5Al-3Ca-0.3Mn	0.1	300	12:1	420 ± 8	451 ± 5	4.1 ± 0.5	(Ref 48)
Mg-6Al-3Ca-0.3Mn				389 ± 6	423 ± 3	3.6 ± 0.3	
Mg-7Al-3Ca-0.3Mn				360 ± 8	414 ± 2	4.4 ± 0.4	
Mg-2Al-2.0Ca	3	400	16:1	251.97 ± 2.0	271 ± 2.2	10.3 ± 0.7	(Ref 49)
Mg-3Al-2.0Ca				244.3 ± 4.2	276.7 ± 5.2	11.2 ± 0.4	
Mg-5Al-2.0Ca				231.1 ± 2.4	296.5 ± 1.1	12.7 ± 2	
Mg-4Al-3Ca-0.3Mn	0.1	350	20:1	331	349	8.2	(Ref 50)
Mg-0.27Al-0.13Ca-0.21Mn	1	500	20:1	170	220	15.5	(Ref 51)
Mg-4Al-2Sr-0.3Mn		360	9:1	262.4	296.4	6.2	(Ref 52)
Mg-4Al-2Sr-1Ca-0.3Mn				299.1	326.7	3.6	
AZ91-3Sn		300	36:1	273	379	7.7	(Ref 40)
Mg-8Al-0.5Zn	0.1	250	20:1	328 ± 2	369 ± 1	4.7 ± 0.2	(Ref 53)
Mg-8Al-4Sn-2Zn				371 ± 2	415 ± 2	9.1 ± 0.1	
AZ62	1	250	25:1	172	313	26.9	(Ref 54)
AZ62-2Sn				179	320	25.3	
AZ62-4Sn				188	330	23.7	
AZ62-8Sn				206	332	13.4	

Table 5 continued

Alloy	Extrusion parameters			Tensile Properties			References
	Ram speed, mm/s	Temp., °C	Extrusion ratio	TYS, MPa	UTS, MPa	El, %	
AZ31	0.1	250	20:1	189	274	24.9	(Ref 55)
		300		154	360	23.9	
	1	300		137	250	23.1	
	2	300		137	246	21.7	
	2	400		154	244	15.7	
AZ31-10 Sn	0.1	250	20:1	319	358	6.1	
		300		289	353	9.1	
	1	300		241	339	14.5	
	2	300		228	329	13.3	
	2	400		214	315	11.0	
AZ31-10 Sn-0.1Na	0.1	300	20:1	336	362	3.1	
		300		292	331	4.4	
	400	232		304	6.9		
AZ91 (E1 alloy)	1	400	4:1	325	364	4.3	Present work
AZ91-1 Ca- 0.9 Sr (E4 alloy)				376	401	1.6	

The bold values represent the developed extruded alloys in the present work, including their extrusion parameters and the corresponding mechanical properties obtained

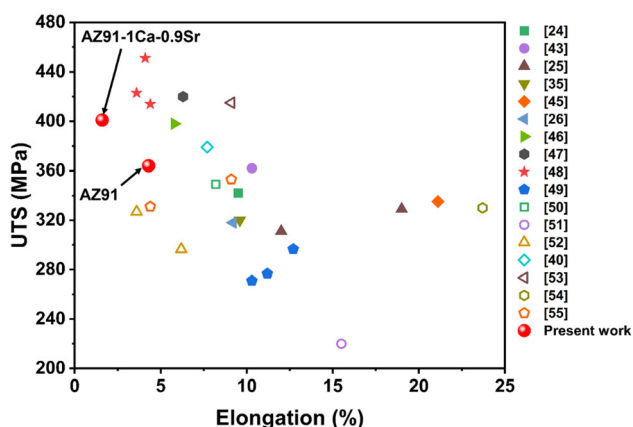


Fig. 14 Comparison of ultimate tensile strength (UTS) of extruded base AZ91 and extruded AZ91-1Ca-0.9Sr alloy developed in the present work with previously reported extruded AZ series alloys

- (1) Extruded microstructure of AZ91 shows the bimodal structure consisting of DDRX grains and deformed grains, whereas extruded microstructures of AZ91-1Ca-xSr alloys show fully recrystallized grains consisting of intermetallic Al-Ca and Al-Sr stringers elongated in the extrusion direction. Thermodynamic calculations predict the stability of these precipitates at 400 °C extrusion temperatures, actively participating in recrystallization. The precipitates are found to be discontinuous in alloys with 0.3% Sr and 0.6% Sr while they form continuous necklace-like structure of stringers in 0.9% Sr and 1.2% Sr alloys. Recrystallization occurs at the boundaries of parent grains as well as around the stringers.
- (2) The average grain size is observed to be reduced with combined incorporation of Ca and Sr to AZ91 after extrusion. The reduction in the grain size of extruded AZ91-1Ca-xSr alloys compared to base alloy is attributed to the grain boundary pinning mechanism due to secondary Al₂Ca and Al₄Sr phases.

- (3) In extruded base AZ91 alloy, new grains formed near deformed grains undergo recrystallization through the grain boundary bulging mechanism. In AZ91-1Ca-xSr alloys, new grains associated with Al-Ca and Al-Sr stringers undergo recrystallization through the particle-stimulated nucleation (PSN), while grains away from stringers recrystallize either via the grain boundary bulging or DDRX mechanism.
- (4) Combined additions of Ca and Sr lead to texture weakening of extruded AZ91 alloy. The Al₂Ca and Al₄Sr precipitates within AZ91-1Ca-xSr extrusions serve as sites for the initiation of the PSN mechanism by inducing local variations in strain energy. PSN, in response, generates nuclei with random orientations, ultimately leading to a reduction in the overall texture sharpness.
- (5) Grain size reduction and precipitate strengthening are mainly responsible for enhancement of strength of extruded AZ91-1Ca-xSr alloys. The reduction in yield asymmetry observed in the AZ91-1Ca-xSr alloys can be ascribed to the collective impacts of grain size reduction and weakened texture resulting from PSN mechanism promoted by Al₂Ca and Al₄Sr intermetallic.
- (6) E4 alloy (AZ91-1 wt.% Ca-0.9 wt.% Sr) exhibits the highest tensile strength in this study, surpassing the majority of the developed extruded AZ series alloys with various alloy additions. Furthermore, E5 alloy (AZ91-1 wt.% Ca-1.2 wt.% Sr) demonstrates the highest compressive strength and exhibits high fracture strain, standing at a very good position among all developed extruded AZ series Mg alloys with alloy additions. Compared to the literature on individual Ca and Sr additions to extruded AZ91, the combined addition of Ca and Sr to extruded AZ91 yields superior tensile and compressive properties. Hence, the extruded AZ91-1Ca-0.9Sr and AZ91-1Ca-1.2Sr alloys developed in the present work emerge as promising candidates for structural applications, particularly when compared to previously developed extruded AZ series Mg alloys.

Table 6 Compressive properties comparison with the available literature

Alloy	Extrusion parameters			Compressive properties			References
	Ram speed, mm/s	Temp., °C	Extrusion ratio	CYS, MPa	UCS, MPa	Fracture strain, %	
AZ91	...	340	25:1	183 ± 4	406 ± 3	15.5 ± 0.3	(Ref 41)
AZ80	1	250	8:1	229 ± 12	(Ref 39)
		300		187 ± 7	
		350		147 ± 0	
Mg-3.6Al-3.3Ca-0.4Mn	0.1	350	20:1	350	~ 510	~ 9.9	(Ref 47)
Mg-4Al-3Ca-0.3Mn	0.1	350	20:1	285	472	9.5	(Ref 50)
AZ31-0.4Sr	...	250	18:1	~ 132	~ 524	...	(Ref 56)
AZ31-0.8Sr	...	250		~ 139	~ 525	...	
AZ31-0.4Sr	...	350		~ 123	~ 450	...	
AZ31-0.8Sr	...	350		~ 121	~ 430	...	
Mg-8Al-0.5Zn	0.1	250	20:1	311 ± 1	433 ± 4	10.2	(Ref 53)
Mg-8Al-4Sn-2Zn				378 ± 2	448 ± 5	9	
AZ31	0.1	250	20:1	184	431	15.1	(Ref 55)
		300		132	386	16.4	
	1	300		121	379	16.2	
	2	300		106	368	17	
	2	400		95	354	17	
AZ31-10 Sn	0.1	250		318	523	10.8	
		300		284	507	11	
	1	300		266	495	11.4	
	2	300		246	476	11.2	
	2	400		206	487	11.2	
AZ31-10 Sn-0.1Na	0.1	300		317	532	9.1	
	2	300		284	529	10.4	
		400		209	442	9.3	
AZ91 (E1 alloy)	1	400	4:1	221	510	14.85	Present work
AZ91-1 Ca- 1.2 Sr (E5 alloy)				282	534	13.11	

The bold values represent the developed extruded alloys in the present work, including their extrusion parameters and the corresponding mechanical properties obtained

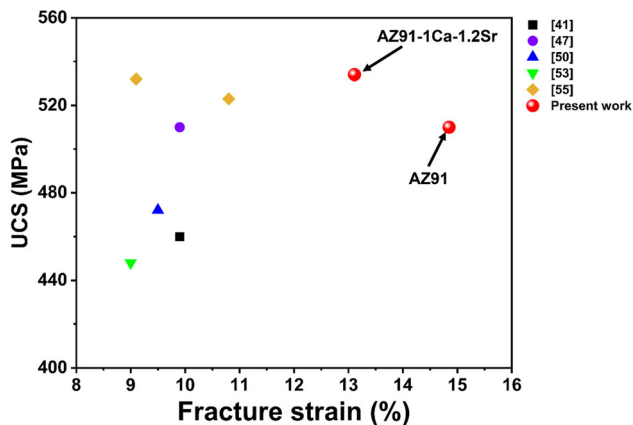


Fig. 15 Comparison of ultimate compressive strength (UCS) of extruded base AZ91 and extruded AZ91-1Ca-1.2Sr alloy developed in the present work with previously reported extruded AZ series alloys

Acknowledgment

Prof. Hemant Borkar would like to acknowledge the ACMS facility at IIT Kanpur, India, for providing the facilities for bulk texture and mechanical properties analysis.

Author's Contributions

Ankush S. Marodkar was involved in writing-original draft, conceptualization, data curation, methodology, formal analysis, investigation and visualization. Vivek Kumar Sahu was responsible for validation, formal analysis, and reviewing and editing. Hemant Borkar participated in supervision, writing-reviewing and editing, project administration, conceptualization and resources.

Conflict of interest

The authors declare that they have no known competing financial interests or personal relationships that could have appeared to influence the work reported in this paper.

References

1. W. Zhang, S. Wang, J. Pan, and J. Yang, Extraordinary Bending Formability of Mg 2.5Nd-0.5Zn-0.5Zr Alloy Sheet through Pulsed Current, *Met. Mater. Int.*, 2023, **29**, p 3371–3384. <https://doi.org/10.1007/s12540-023-01450-6>
2. H. Abedi, M. Emamy, J. Rassizadehghani, and H. Mirzadeh, Synergistic Effects of Cerium-Based Rare Earth Addition and Hot Deformation on the Microstructure and Mechanical Properties of Mg-0.5Zn-0.5Zr Magnesium Alloy, *Met. Mater. Int.*, 2022, **28**, p 1105–1113. <https://doi.org/10.1007/s12540-021-01065-9>
3. J. Bohlen, S.B. Yi, J. Swiostek, D. Letzig, H.G. Brokmeier, and K.U. Kainer, Microstructure and Texture Development during Hydrostatic

- Extrusion of Magnesium Alloy AZ31, *Scr. Mater.*, 2005, **52**, p 259–264. <https://doi.org/10.1016/j.scriptamat.2005.03.036>
4. M.R. Barnett, M.D. Nave, and C.J. Bettles, Deformation Microstructures and Textures of Some Cold Rolled Mg Alloys, *Mater. Sci. Eng. A*, 2004, **386**(1–2), p 205–211. <https://doi.org/10.1016/j.msea.2004.07.030>
 5. F. Kong, H. Feng, H. Chen, Y. Lin, Y. Wang, W. Xie, G. Wei, Y. Yang, and X. Peng, Non-basal Slips Mediated Dynamic Recrystallization Promote Synergistic Strengthening and Toughening of Centrifugal Casting Mg-1.1Mn-0.5Al Alloy via High Strain Rolling, *Met. Mater. Int.*, 2023, **2**, p 2. <https://doi.org/10.1007/s12540-023-01516-5>
 6. M. Panchal, K.R. Ravi, L. Kaushik, R. Khatirkar, S. Choi, and J. Singh, Texture Control Techniques for Improving Room Temperature Formability of Mg Alloys including Pre-twinning: A Review, *Met. Mater. Int.*, 2023, **29**, p 3471–3489. <https://doi.org/10.1007/s12540-023-01472-0>
 7. J. Kim, K. Yoo, and J. Byeon, Tension Twin-Induced Premature Fracture Mechanism of Aging-Treated AZ91D Magnesium Alloy, *Mater. Charact.*, 2021, **172**, 110865. <https://doi.org/10.1016/j.matchar.2020.110865>
 8. O. Muransky, M.R. Barnett, V. Luzin, and S. Vogel, On the Correlation Between Deformation Twinning and Lüders-Like Deformation in an Extruded Mg Alloy: In Situ Neutron Diffraction and EPSC4 Modelling, *Mater. Sci. Eng. A*, 2010, **527**, p 1383–1394. <https://doi.org/10.1016/j.msea.2009.10.018>
 9. Y.N. Wang and J.C. Huang, The Role of Twinning and Untwinning in Yielding Behavior in Hot-Extruded Mg-Al-Zn Alloy, *Acta Mater.*, 2007, **55**, p 897–905. <https://doi.org/10.1016/j.actamat.2006.09.010>
 10. Q. Liao, W. Hu, Q. Le, X. Chen, and Y. Jiang, Improvement of Yield Asymmetry and Enhancement of Mechanical Properties of Extruded AZ110 Alloy with La-Rich Misch Metal Addition, *Met. Mater. Int.*, 2022, **28**, p 1143–1156. <https://doi.org/10.1007/s12540-021-00978-9>
 11. S.R. Agnew and O. Duygulu, Plastic Anisotropy and the Role of Non-basal Slip in Magnesium Alloy AZ31B, *Int. J. Plast.*, 2005, **21**, p 1161–1193. <https://doi.org/10.1016/j.ijplas.2004.05.018>
 12. M.A. Meyers, O. Vöhringer, and V.A. Lubarda, The Onset of Twinning in Metals: A Constitutive Description, *Acta Mater.*, 2001, **49**, p 4025. [https://doi.org/10.1016/S1359-6454\(01\)00300-7](https://doi.org/10.1016/S1359-6454(01)00300-7)
 13. J.F. Brown, Magnesium Extrusion: Properties, Applications, and Alloy Development, *Light Metal Age-Chicago*, 2007, **65**(2), p 6–10
 14. J.W. Senn and S.R. Agnew, *Texture Randomization during Thermo-mechanical Processing of a Magnesium-Yttrium-Neodymium Alloy*, Metallurgical Society of CIM, Montreal Canada, 2006, p 115–130
 15. E. Ball and P.B. Prangnell, Tensile-Compressive Yield Asymmetries in High Strength Wrought Magnesium Alloys, *Scr. Metall.*, 1994, **31**(2), p 111–116. [https://doi.org/10.1016/0956-716X\(94\)90159-7](https://doi.org/10.1016/0956-716X(94)90159-7)
 16. N. Stanford and M.R. Barnett, The Origin of ‘Rare Earth’ Texture Development in Extruded Mg-Based Alloys and Its Effect on Tensile Ductility, *Mater. Sci. Eng. A*, 2008, **496**(1–2), p 399–408. <https://doi.org/10.1016/j.msea.2008.05.045>
 17. J.D. Robson, A.M. Twier, G.W. Lorimer, and P. Rogers, Effect of Extrusion Conditions on Microstructure, Texture, and Yield Asymmetry in Mg-6Y-7Gd-0.5 wt% Zr Alloy, *Mater. Sci. Eng. A*, 2011, **528**(24), p 7247–7256. <https://doi.org/10.1016/j.msea.2011.05.075>
 18. T. Brownsmith, J.D. Robson, M. Turski, and A. Beer, The influence of extrusion conditions on the microstructure and texture of a Mg-4Y-3RE alloy, in *10th International Conference on Mg Alloys and Their Applications*, 2015, p 459–467
 19. N. Stanford, R.K.W. Marceau, and M.R. Barnett, The Effect of High Yttrium Solute Concentration on the Twinning Behaviour of Magnesium Alloys, *Acta Mater.*, 2015, **82**, p 447–456. <https://doi.org/10.1016/j.actamat.2014.09.022>
 20. F. Bu, Q. Yang, X. Qiu, T. Zheng, D. Zhang, X. Niu, Y. Li, X. Liu, and J. Meng, Study on the Assemblage of Y and Gd on Microstructure and Mechanical Properties of Hot Extruded Mg–Al–Zn alloy, *Mater. Sci. Eng. A*, 2015, **639**, p 198–207. <https://doi.org/10.1016/j.msea.2015.05.008>
 21. N. Stanford, The Effect of Calcium on the Texture, Microstructure and Mechanical Properties of Extruded Mg-Mn-Ca Alloys, *Mater. Sci. Eng. A*, 2010, **528**(1), p 314–322. <https://doi.org/10.1016/j.msea.2010.08.097>
 22. C. Singh, R.L. Narayan, and J. Jain, Influence of Simultaneous Alloying with Ca and Sc on the High Temperature Deformation Mechanism, Texture, and Recrystallization Behavior of Mg-Ca-Sc Alloys, *Mater. Charact.*, 2021, **179**, 111343. <https://doi.org/10.1016/j.matchar.2021.111343>
 23. S.H. Allameh and M. Emamy, The Effect of Ca Content on the Microstructure, Hardness and Tensile Properties of AZ81 Mg Cast Alloy, *J. Mater. Eng. Perform.*, 2017, **26**, p 2151–2161. <https://doi.org/10.1007/s11665-017-2671-1>
 24. F. Li, W.Y. Peh, V. Nagarajan, M.K. Ho, A. Danno, B.W. Chua, and M.J. Tan, Development of Non-flammable High Strength AZ91+Ca Alloys via Liquid Forging and Extrusion, *Mater. Des.*, 2016, **99**, p 37–43. <https://doi.org/10.1016/j.matdes.2016.03.014>
 25. S.H. Allameh, M. Emamy, E. Maleki, and B. Pourbahari, Effect of microstructural Refinement on Tensile Properties of AZ80 Magnesium Alloy via Ca Addition and Extrusion Process, *Proc. Mater. Sci.*, 2015, **11**, p 89–94. <https://doi.org/10.1016/j.mspro.2015.11.115>
 26. C. Che, Z. Cai, X. Yang, L. Cheng, and Y. Du, The Effect of Co-Addition of Si, Ca and RE on Microstructure and Tensile Properties of As-Extruded AZ91 Alloy, *Mater. Sci. Eng. A*, 2017, **705**, p 282–290. <https://doi.org/10.1016/j.msea.2017.08.026>
 27. H. Borkar, M. Hoseini, and M. Peguleryuz, Effect of Strontium on the Texture and Mechanical Properties of Extruded Mg-1% Mn Alloys, *Mater. Sci. Eng. A*, 2012, **549**, p 168–175. <https://doi.org/10.1016/j.msea.2012.04.029>
 28. A. Sadeghi, M. Hoseini, and M. Peguleryuz, Effect of Sr Addition on Texture of Mg-3Al-1Zn (AZ31) Alloy during Extrusion, *Mater. Sci. Eng. A*, 2011, **528**, p 3096–3104. <https://doi.org/10.1016/j.msea.2010.12.091>
 29. A. Galiyev, R. Kaibyshev, and G. Gottstein, Correlation of Plastic Deformation and Dynamic Recrystallization in Magnesium Alloy ZK60, *Acta Mater.*, 2001, **49**, p 1199–1207. [https://doi.org/10.1016/S1359-6454\(01\)00020-9](https://doi.org/10.1016/S1359-6454(01)00020-9)
 30. O. Sitdikov and R. Kaibyshev, Dynamic Recrystallization in Pure Magnesium, *Mater. Trans.*, 2001, **42**(9), p 1928–1937. <https://doi.org/10.2320/matertrans.42.1928>
 31. C. Bettles and M. Barnett, *Advances in Wrought Magnesium Alloys: Fundamentals of Processing, Properties and Applications*, Woodhead Publishing, Philadelphia, 2012
 32. A. Chapuis and J.H. Driver, Temperature Dependency of Slip and Twinning in Plane Strain Compressed Magnesium Single Crystals, *Acta Mater.*, 2011, **59**, p 1986–1994. <https://doi.org/10.1016/j.actamat.2010.11.064>
 33. A.S. Marodkar, H. Patil, H. Borkar, and A. Behl, Effect of Squeeze Casting and Combined Addition of Calcium and Strontium on Microstructure and Mechanical Properties of AZ91 Magnesium Alloy, *Int. J. Met.*, 2023, **17**, p 2252–2270. <https://doi.org/10.1007/s40962-022-00943-1>
 34. H. Watanabe, M. Yamaguchi, Y. Takigawa, and K. Higashi, Mechanical Properties of Mg-Al-Ca Alloy Processed by Hot Extrusion, *Mater. Sci. Eng. A*, 2007, **454**, p 384–388. <https://doi.org/10.1016/j.msea.2006.12.130>
 35. G. Shao-Kang, Z. Shi-Jie, W. Li-Guo, Y. Qing, and C. Wen-bo, Microstructures and Mechanical Properties of Double Hot-Extruded AZ80+xSr Wrought Alloys, *Trans. Nonferrous Met. Soc. China*, 2007, **17**(6), p 1143–1151
 36. I. Gokalp and A. Incesu, Effect of Ca Addition to the Elevated Temperature Mechanical Properties of AZ Series Magnesium Alloys, *Int. J. Met.*, 2023, **17**, p 1402–1412. <https://doi.org/10.1007/s40962-022-00872-z>
 37. F. Hehmann, F. Sommer, and B. Predel, Extension of Solid Solubility in Magnesium by Rapid Solidification, *Mater. Sci. Eng. A*, 1990, **125**, p 249–265. [https://doi.org/10.1016/0921-5093\(90\)90175-3](https://doi.org/10.1016/0921-5093(90)90175-3)
 38. H. Borkar, R. Gauvin, and M. Peguleryuz, Effect of Extrusion Temperature on Texture Evolution and Recrystallization in Extruded Mg-1% Mn and Mg-1% Mn-1.6%Sr Alloys, *J. Alloys Compd.*, 2013, **555**, p 219–224. <https://doi.org/10.1016/j.jallcom.2012.12.078>
 39. S. Kim, S.W. Lee, B.G. Moon, H.S. Kim, and S.H. Park, Variation in Dynamic Deformation Behavior and Resultant Yield Asymmetry of AZ80 Alloy with Extrusion Temperature, *J. Mater. Sci. Technol.*, 2020, **46**, p 225–236. <https://doi.org/10.1016/j.jmst.2019.11.033>
 40. K. Wu, J. Yeh, and S. Chang, Refined Microstructure and Improved Mechanical Properties of High-Ratio Extruded AZ91–xSn Magnesium Alloy, *Mater. Chem. Phys.*, 2015, **162**, p 757–763. <https://doi.org/10.1016/j.matchemphys.2015.06.052>
 41. Y. Zhu, F. Liu, R. Xin, B. Song, and Q. Liu, Influence of Aging Prior to Extrusion on the Microstructure and Mechanical Properties of an

- Extruded AZ91 Alloy, *Adv. Eng. Mater.*, 2020, **22**(7), p 2000201. <https://doi.org/10.1002/adem.202000201>
42. H. Ding, L. Liu, S. Kamado, W. Ding, and Y. Kojima, Study of the Microstructure, Texture and Tensile Properties of As-Extruded AZ91 Magnesium Alloy, *J. Alloys Compd.*, 2008, **456**(1–2), p 400–406. <https://doi.org/10.1016/j.jallcom.2007.02.045>
 43. X. Huang, Y. Chino, M. Yuasa, H. Ueda, M. Inoue, F. Kido, and T. Matsumoto, Microstructure and Mechanical Properties of AZX912 Magnesium Alloy Extruded at Different Temperatures, *Mater. Sci. Eng. A*, 2017, **679**, p 162–171. <https://doi.org/10.1016/j.msea.2016.10.032>
 44. D. Zhao, Z. Wang, M. Zuo, and H. Geng, Effects of Heat Treatment on Microstructure and Mechanical Properties of Extruded AZ80 Magnesium Alloy, *Mater. Des. (1980-2015)*, 2014, **56**, p 589–593. <https://doi.org/10.1016/j.matdes.2013.11.072>
 45. A. Afsharnaderi, M. Lotfpour, H. Mirzadeh, M. Emamy, and M. Malekan, Enhanced Mechanical Properties of As-Cast AZ91 Magnesium Alloy by Combined RE-Sr Addition and Hot Extrusion, *Mater. Sci. Eng. A*, 2020, **792**, 139817. <https://doi.org/10.1016/j.msea.2020.139817>
 46. S. Kim, S.W. Lee, B.G. Moon, H.S. Kim, Y.M. Kim, and S.H. Park, Influence of Extrusion Temperature on Dynamic Deformation Behaviors and Mechanical Properties of Mg-8Al-0.5 Zn-0.2 Mn-0.3 Ca-0.2 Y Alloy, *J. Mater. Res. Technol.*, 2019, **8**(6), p 5254–5270. <https://doi.org/10.1016/j.jmrt.2019.08.048>
 47. S.W. Xu, K. Oh-ishi, S. Kamado, F. Uchida, T. Homma, and K. Hono, High-Strength Extruded Mg-Al-Ca-Mn Alloy, *Scr. Mater.*, 2011, **65**(3), p 269–272. <https://doi.org/10.1016/j.scriptamat.2011.04.026>
 48. Z.T. Li, X.G. Qiao, C. Xu, S. Kamado, M.Y. Zheng, and A.A. Luo, Ultrahigh Strength Mg-Al-Ca-Mn Extrusion Alloys with Various Aluminum Contents, *J. Alloys Compd.*, 2019, **792**, p 130–141. <https://doi.org/10.1016/j.jallcom.2019.03.319>
 49. L. Zhang, K. Deng, K. Nie, F. Xu, K. Su, and W. Liang, Microstructures and Mechanical Properties of Mg-Al-Ca Alloys Affected by Ca/Al ratio, *Mater. Sci. Eng. A*, 2015, **636**, p 279–288. <https://doi.org/10.1016/j.msea.2015.03.100>
 50. T. Homma, S. Hirawatari, H. Sunohara, and S. Kamado, Room and Elevated Temperature Mechanical Properties in the As-Extruded Mg-Al-Ca-Mn Alloys, *Mater. Sci. Eng. A*, 2012, **539**, p 163–169. <https://doi.org/10.1016/j.msea.2012.01.074>
 51. T. Nakata, T. Mezaki, R. Ajima, C. Xu, K. Oh-Ishi, K. Shimizu, S. Hanaki, T.T. Sasaki, K. Hono, and S. Kamado, High-Speed Extrusion of Heat-Treatable Mg-Al-Ca-Mn Dilute Alloy, *Scr. Mater.*, 2015, **101**, p 28–31. <https://doi.org/10.1016/j.scriptamat.2015.01.010>
 52. J. Bai, S. Yangshan, X. Feng, X. Shan, Q. Jing, and T. Weijian, Effect of Extrusion on Microstructures, and Mechanical and Creep Properties of Mg-Al-Sr and Mg-Al-Sr-Ca Alloys, *Scr. Mater.*, 2006, **55**(12), p 1163–1166. <https://doi.org/10.1016/j.scriptamat.2006.08.020>
 53. S.H. Park, J. Jung, Y.M. Kim, and B.S. You, A New High-Strength Extruded Mg-8Al-4Sn-2Zn Alloy, *Mater. Lett.*, 2015, **139**, p 35–38. <https://doi.org/10.1016/j.matlet.2014.10.033>
 54. S.W. Bae, S. Kim, J.U. Lee, W. Jo, W. Hong, W. Kim, and S.H. Park, Improvement of Mechanical Properties and Reduction of Yield Asymmetry of Extruded Mg-Al-Zn Alloy through Sn Addition, *J. Alloys Compd.*, 2018, **766**, p 748–758. <https://doi.org/10.1016/j.jallcom.2018.07.028>
 55. F.R. Elsayed, T.T. Sasaki, T. Ohkubo, H. Takahashi, S.W. Xu, S. Kamado, and K. Hono, Effect of Extrusion Conditions on Microstructure and Mechanical Properties of Microalloyed Mg-Sn-Al-Zn Alloys, *Mater. Sci. Eng. A*, 2013, **588**, p 318–328. <https://doi.org/10.1016/j.msea.2013.09.050>
 56. K. Hazeli, A. Sadeghi, M.O. Pekguleryuz, and A. Kontsos, The Effect of Strontium in Plasticity of Magnesium Alloys, *Mater. Sci. Eng. A*, 2013, **578**, p 383–393. <https://doi.org/10.1016/j.msea.2013.04.101>

Publisher's Note Springer Nature remains neutral with regard to jurisdictional claims in published maps and institutional affiliations.

Springer Nature or its licensor (e.g. a society or other partner) holds exclusive rights to this article under a publishing agreement with the author(s) or other rightsholder(s); author self-archiving of the accepted manuscript version of this article is solely governed by the terms of such publishing agreement and applicable law.